International Journal of Thermal Sciences 89 (2015) 327–336

Contents lists available at ScienceDirect

International Journal of Thermal Sciences

journal homepage: www.elsevier.com/locate/ijts

Study on the thermal behaviors of power lithium iron phosphate (LFP) aluminum-laminated battery with different tab configurations

Shuanglong Du [a], Ming Jia [a, b, *], Yun Cheng [a], Yiwei Tang [a], Hongliang Zhang [a], Lihua Ai [b], Kai Zhang [a], Yanqing Lai [a]

[a] School of Metallurgy and Environment, Central South University, Changsha 410083, PR China
[b] Hunan Aihua Group Co., Ltd, Yiyang 413002, PR China

ARTICLE INFO

Article history:
Received 9 May 2014
Received in revised form
19 November 2014
Accepted 20 November 2014
Available online 18 December 2014

Keywords:
Lithium-ion battery
Tab configurations
Temperature distributions

ABSTRACT

The thermal response of the battery is one of the key factors affecting the performance and life span of lithium iron phosphate (LFP) batteries. A 3.2 V/10 Ah LFP aluminum-laminated batteries are chosen as the target of the present study. A three-dimensional thermal simulation model is established based on finite element theory and proceeding from the internal heat generation of the battery. The study illustrates a three-dimensional relationship among the total internal heat generation rate of the battery, the discharge rate of the battery, and the depth of discharge. The effects on the heat distribution of the battery cells by different types of tab distributions are also explored. Results show that the thermal behavior of the discharge process can be effectively simulated with the Bernardi equation, by coupling the dynamic changes of the battery temperature, internal resistance and voltage temperature coefficient. The interior chemical reversible heat of the battery is manifested by the endothermic process when DOD (Depth of Discharge) is smaller than 0.7 and by the exothermic process when DOD is larger than 0.7. The irreversible heat takes an increasingly dominant role with the increase of discharge rate; under the condition of high-rate discharge, batteries with a single-side tab distribution are generally found to have a non-uniform cell temperature distribution, while those with a double-side tab distribution have improved cell temperature distributions. Widening the tabs can also greatly reduce the maximum temperature of the cell.

1. Introduction

Lithium-ion batteries feature high working voltages, high energy densities, long life spans and low self-discharge rates, and thus have been widely applied in high-power applications [1]. However, Li-ion batteries have thermal performance issues that cannot be ignored. Heat will accumulate in limited space if it cannot be dissipated in a timely fashion, thereby causing continuous rising of a battery's operating temperature; if the temperature rises higher than 50 °C, the battery's chemical performance and cycle life will be significantly reduced [2]. The operational process of a battery requires both electrochemical consistency and temperature uniformity among the battery cells. To ensure high battery performance, it is necessary to implement relevant and effective thermal management strategies. Although there are a wide variety of thermal management strategies for batteries, there are two primary categories [3]: (a) an external attached cooling design, including air cooling, oil cooling and phase-change material cooling, and (b) an internal design change of the battery itself in order to reduce its heat generation rate or improve its heat dissipation rate, such as changing the battery structure and tab design.

Battery design can be guided by adopting the currently fast-developing computer numerical simulation technology. By combining the related theory of heat transfer and establishing the electro-thermal model of batteries, numerical simulation can shorten the design cycle, by gaining time and cutting costs. Bernardi D [4] comprehensively considered the electrochemical reaction heat, Joule heating, heat of mixing, and phase-change-related heat generation, and put forward the currently widely-applied thermal model of batteries through thermodynamic calculation. Using this model as a basis, Wencheng L [5]studied the discharge behavior of LFP batteries at an rate smaller than 3C. They found that

* Corresponding author. School of Metallurgy and Environment, Central South University, Changsha 410083, PR China.
E-mail address: jiamingsunmoon@aliyun.com (M. Jia).

http://dx.doi.org/10.1016/j.ijthermalsci.2014.11.018
1290-0729/

at such low rates the temperature drop on the surface of the battery was mainly due to the reversible reaction heat. Additionally they concluded, based on calculation, that it was reasonable to ignore the heat of mixing and the side reaction chemical heat. To apply the traditional thermal model of Bernardi D [4] to an actual heat generation study of batteries and to ignore the terms with negligible contributions to the heat generation rate can provide calculation precision, and lay a reliable foundation of battery thermal design. This has been verified by our research group in previous studies [6–9].

Compared with the traditional experimental verification, numerical simulation has been shown to be unparalleled in its superiority as a battery thermal design technique. Chee BS [10–12] used the ideas of finite element to conduct a simulation of battery electrode slice layers and explored the influence of the length-width ratio of electrode slices, tab size and environmental temperature on the current distribution and potential distribution of the electrode slices. The study showed that the batteries' structural design influences the current distribution and potential distribution of electrode slices. Zhao W [13] established a three-dimensional electrochemical model and studied in great detail the influence of the distribution of electrodes and tabs of coiled ternary batteries on the current and potential distributions of the battery current collector. Zhao W deemed that to adopt the configuration of multiple tabs could effectively give play to the energy density of the battery, and improve the availability of active materials. These studies show that the influence of electrode slice design, tab design and working environmental temperature on battery performance by means of numerical calculation can dramatically improve the study efficiency, and also provide theoretic guidance to battery manufacture and design. However, most current researchers focus on the study of batteries with lithium cobalt oxide and lithium manganate anodes, or ternary system lithium-ion batteries. This results in much less focus on the field of LFP batteries, which have gradually become widely applied especially in electric vehicles (EV) application [14]. With the progress of technology, it is of both theoretical and practical significance to probe the influence of battery design on the temperature distribution and performance of batteries from the perspective of heat generation within the batteries.

The 3.2 V/10 Ah LFP aluminum-laminated batteries are chosen as the target of the present study. By establishing a three-dimensional thermal simulation model based on finite element theory and proceeding from the heat generation inside the battery, the study discusses in detail the evolution of different heat generation mechanisms during the batteries' dissipation process, and probes into the cell temperature distributions of batteries with different tab designs. The result of the study can provide relevant theoretical guidance for an optimized design and thermal management of LFP power batteries.

Table 1
Parameters of lithium ion battery cell.

Capacity (Ah)	Mass (g)	Density (kg m^{-3})	Voltage (V)	Width (mm)	Thickness (mm)	Height (mm)
10	259.64	1881.45	3.2	100	12	115

2. Simulation and calculation

2.1. Simulation object

3.2 V/10 Ah LFP aluminum-laminated batteries are selected as the study object. Fig. 1 displays the cells of lithium-ion battery; the basic parameters of LFP battery cells can be seen in Table 1.

2.2. Modeling

The interior of the battery with an evenly distributed internal heat source is taken as a temperature field and the influence of the interior convection and surface radiation of the battery on the cell temperature is ignored. The calculation is conducted by establishing the energy transport equation and introducing the boundary condition and initial condition, thus the temperature field distribution inside the battery is calculated [15]. Assuming that the battery cell can be fully discharged theoretically (i.e., the discharge rate is N C, and the discharge duration is 3600/N s), the current conditions are respectively 1C, 3C, 5C, and 10C, with an initial temperature of 300 K.

The essence of thermal simulation of the battery is in its internal energy conservation of the battery, as shown in Equation (1):

$$\rho C_p \frac{\partial T}{\partial t} = \lambda_x \frac{\partial^2 T}{\partial x^2} + \lambda_y \frac{\partial^2 T}{\partial y^2} + \lambda_z \frac{\partial^2 T}{\partial z^2} + q \tag{1}$$

where ρ represents the mean density of the battery; C_p represents the mean specific heat of the battery; T represents the temperature; t represents the time; the term of heat source q adopts the expression approach of Thomas KE [16]:

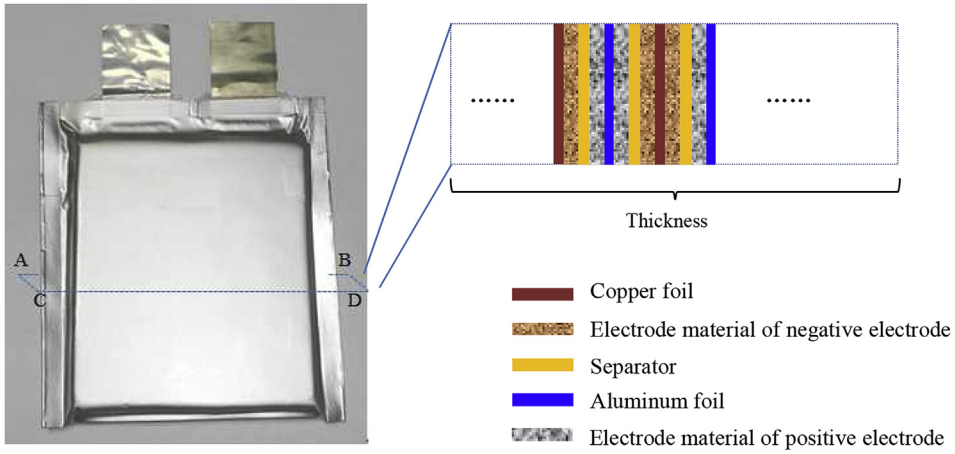

Fig. 1. A sample 3.2 V/10 Ah LFP aluminum-laminated battery.

$$q = I(V - U_{avg}) + IT\frac{\partial U_{avg}}{\partial T} - \sum_i \Delta H_i^{avg} r_i - \int \sum_j \left(\overline{H}_j - \overline{H}_j^{avg}\right)\frac{\partial c_j}{\partial t} dv \quad (2)$$

where I represents the working current; U_{avg} represents the balanced electromotive force; V represents the battery voltage; T represents the battery temperature; dU_{avg}/dT represents the voltage temperature coefficient; ΔH_i^{avg} represents the average enthalpy change of side reaction i; r_i represents the rate constant of side reaction i; $\overline{H}_j$ represents the partial molar enthalpy change of material j; c_j represents the concentration of material j. The first two terms in the equation above represent the irreversible heat generation term and chemical reaction reversible heat generation term, respectively; the third term is the heat generation of the side reaction and the fourth term is the heat generation during material mixing process. Regarding the LFP aluminum-laminated battery, it is required to ignore the battery aging caused by the internal side reaction as well as the heat generation terms during the material mixing process caused by the concentration gradient inside the battery; related processes are consistent with the literature [17].

By ignoring the third and fourth terms of Equation (2), we can obtain the Bernardi equation of heat generation:

$$q = I(U_{avg} - V) - IT\frac{dU_{avg}}{dT} \quad (3)$$

$$Q_{hir} = I(U_{avg} - V) = I^2 R_{cell} \quad (4)$$

$$Q_{hr} = -IT\frac{dU_{avg}}{dT} \quad (5)$$

where (3)–(5): Q_{hir} and Q_{hr} represent the irreversible heat generation rate and chemical reaction reversible heat generation rate caused by the internal resistance change of the battery, respectively; R_{cell} is the internal resistance of the battery. The internal resistance R of the battery in the study is measured by the means of open-circuit voltage [18], and its changing rule obtained by the experiment is shown in Fig. 2. Considering that the voltage is changing with the temperature, the dynamic voltage temperature coefficient is adopted from the literature [5], as shown in Fig. 3.

Strictly speaking, during the battery discharge process the parameters of thermal physical properties at each point shifts due to differences of current densities in the various parts. However, the thermal models currently used adopt the same thermal physical property parameter during the discharge process, and their difference is reflected on the model of heat generation rate [19].

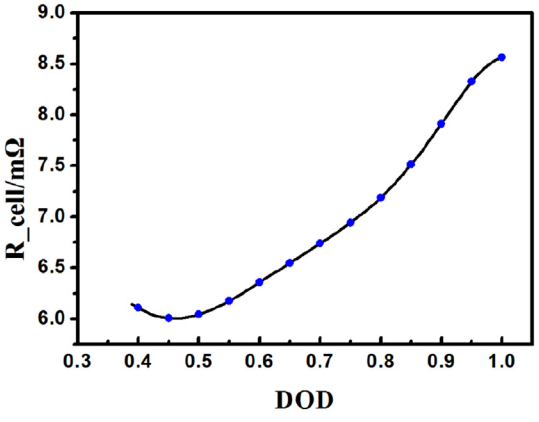

Fig. 2. Internal resistance of battery as a function of DOD.

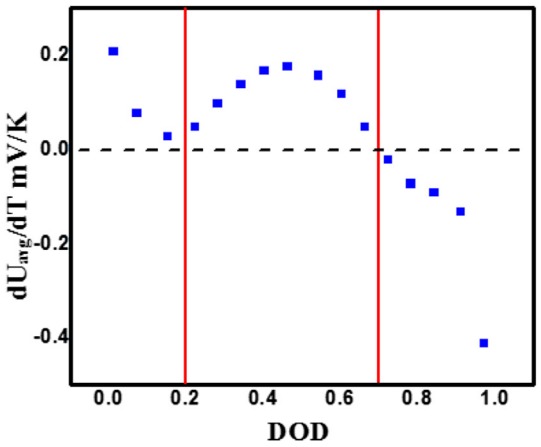

Fig. 3. The parameter dE_{oc}/dT of $LiFePO_4$ battery.

The anode tab of the battery is made of aluminum and its cathode tab is made of copper. During the discharge process, the heat generated by tabs is Joule heat. The calculation equation of heat generation rate is as below:

$$q_{Al,Cu} = \frac{Q_{Al,Cu}}{V_{Al,Cu}} = \frac{I^2 R_{Al,Cu}}{V_{Al,Cu}} \quad (6)$$

$Q_{Al,Cu}$ is the heat generation rate of anode and cathode tabs; $R_{Al,Cu}$ is the resistance of anode and cathode tabs; $V_{Al,Cu}$ is the volume of anode and cathode tabs.

Based on Newton's law of cooling, the boundary condition of the thermal model of LFP battery can be described by Equation (7):

$$\lambda\left(\frac{\partial T}{\partial n}\right) = h(T_{amb} - T_\infty) \quad (7)$$

T_{amb} is the temperature of surrounding fluid; T_∞ is the surface temperature of the battery; λ is the heat conductivity coefficient of the surface material of the battery; n represents the vector direction of vertical battery surface; h is the heat exchange coefficient between the battery surface and surrounding environment. It has been pointed [20] out that under the condition of natural convection the typical value of h is 5 W m^{-2} K^{-1}; under the condition of forced air cooling at a general intensity the typical value of h is 10 W m^{-2} K^{-1}.

Table 2
Thermal–physical properties parameters of the lithium-ion battery materials.

Materials	Density (kg m^{-3})	Specific heat (J kg^{-1} K^{-1})	Heat conductivity coefficient (J m^{-1} K^{-1})
Separator	492.00	1978.16	0.334
Electrode material of positive electrode	1500.00	1260.20	1.48
Electrode material of negative electrode	2660.00	1437.40	1.04
Aluminum foil	2702.00	903.00	238.00
Copper foil	8933.00	385.00	398.00
Aluminum laminate film	1636.000	1376.947	0.427
Tab of positive electrode	2702.000	903.000	238.000
Tab of negative electrode	8933.000	385.000	398.000
Electrolyte	1290.000	133.900	0.450

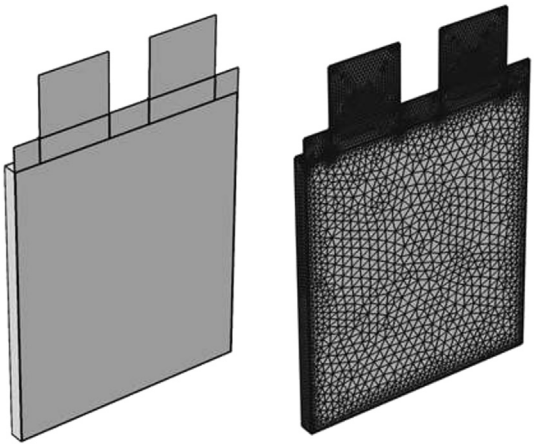

Fig. 4. The three-dimensional model and the meshment.

2.3. Thermophysical parameters

Thermophysical parameters are the basis for the battery simulation process, therefore reliable parameters can exert a significant influence on the accuracy of the simulation result under the working condition. Table 2 lists the thermophysical parameters [21] of each material.

To simplify the calculation, each parameter is considered to be time independent. The mean specific heat capacity of Lithium-ion battery during calculation can be worked out by Equation (8):

$$\rho_{cell}c_{cell} = \frac{\sum \rho_i c_i V_i}{\sum V_i} \tag{8}$$

ρ_{cell} and ρ_i are the mean density of the battery and the density of each material, respectively; c_{cell} and c_i are the mean heat capacity of the battery and the specific heat capacity of each material, respectively; V_i is the volume occupied by each material.

Since lithium-ion batteries are made up of multiple-layers of different materials which are divided by electrolyte, the heat conductivity coefficient of the battery is anisotropic. According to the basic principle of heat transfer, the heat transfer can be divided into heat transfers that are in parallel and in series [15]. The mean heat conductivity coefficient in parallel can be determined by Equation (9) and that in series can be determined by Equation (10).

$$\lambda_x = \lambda_z = \frac{\lambda_p L_{x_p} + \lambda_n L_{x_n} + \lambda_s L_{x_s}}{L_y} \tag{9}$$

$$\lambda_y = \frac{L_y}{\frac{L_{x_p}}{\lambda_p} + \frac{L_{x_n}}{\lambda_n} + \frac{L_{x_s}}{\lambda_s}} \tag{10}$$

λ_x, λ_y and λ_z are the heat conductivity coefficients of the battery materials at the directions of x, y and z, respectively; λ_p, λ_n and λ are,

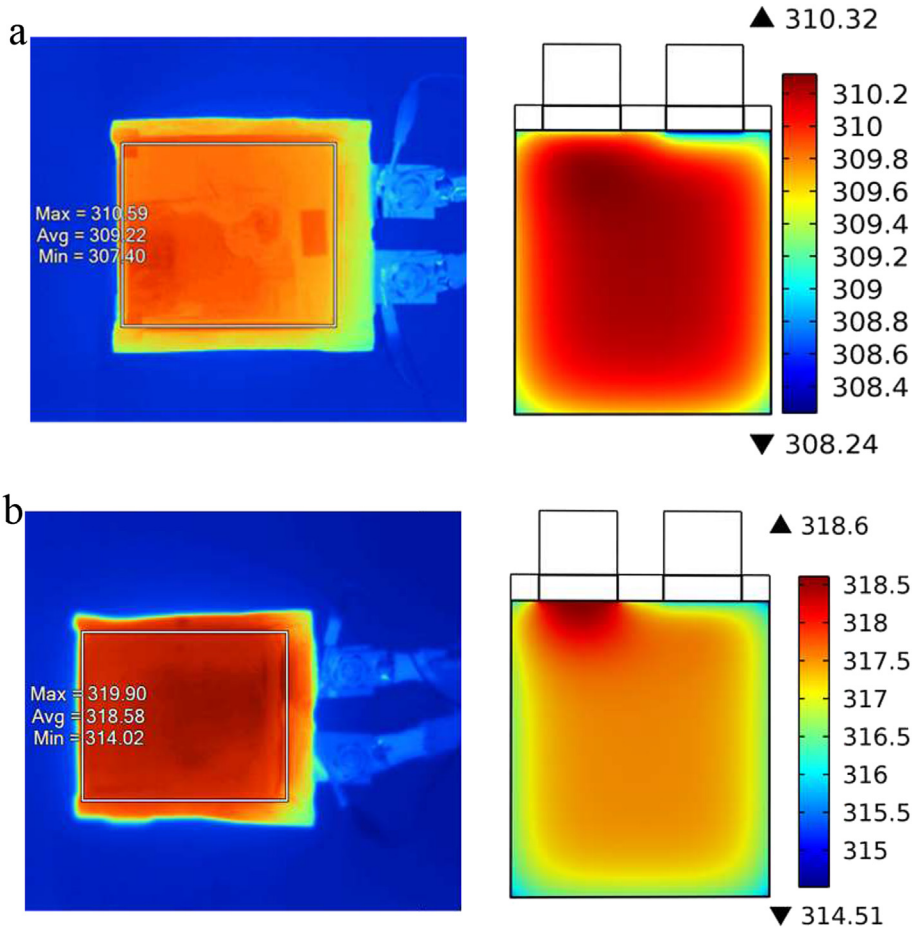

Fig. 5. The contrast of contours between infrared imagery and simulated temperature distribution in natural cooling condition (a) 3C discharge; (b) 5C discharge.

respectively, the anode slice, cathode slice and the heat conductivity coefficient of diagram inside the battery.

3. Results and discussion

3.1. Model verification

10 Ah power LFP batteries are selected as the study object. A three-dimensional model is built below (see Fig. 4) to study its thermal behaviors. We adopt free tetrahedral method using COMSOL Multiphysics Software to mesh and then get 143,462 elements in total.

The experiment adopts the method stipulated in literature [4]. A Guangzhou Qingtian test cabinet (ht-5c200d200-4) was used to test the charge–discharge process of the battery. During the discharge of the battery, Ti55 thermal imager manufactured by FLUKE is used to scan the temperature field on the surface of the battery to obtain the distribution of the temperature field. This battery is designed for high power density, its typical discharge rates are 3C and 5C. Thus Fig. 5 provides the infrared imagery results and simulation results at the discharge end of 3C and 5C at room temperature with natural cooling condition.

As seen in Fig. 5, the infrared results and the simulation results are basically consistent; however, there are two primary differences between them which we discuss in the following. First, the distributions are different in the high-temperature regions. In the high temperature region, while the simulation results appear near the anode tab, the infrared results appear in the opposite direction. This is because both the anode tab and cathode tab are in direct contact with the aluminum connecting plate with good heat conductivity during the large-current discharge test, and thus the heat of the tabs was effectively dissipated. This led to the region near the tabs having a relatively low temperature as compared to the simulation. The second major difference is that the temperature of the cell is more evenly distributed in the simulation. The simulation results show a better temperature uniformity of the battery because the battery is assumed to be made of an idealized and uniform internal active material. However, because of the limits of the actual battery manufacturing process, due to different equipment processes, it is hard to ensure uniform distribution of the internal active materials of the battery. This leads to the difference that is seen between the infrared imagery results and simulation results. On the whole, the battery cell model adopted by the study accurately reflects the thermal behavior of the battery.

3.2. Calculation of heat generation inside the battery

The Bernardi equation is used to calculate the heat generation rate inside the battery by combining the dynamic changes of the battery temperature, internal resistance (Fig. 2) and voltage temperature coefficient (Fig. 3). Fig. 6 provides the curves of irreversible heat generation rate Q_{hir} inside the battery, reversible heat generation rate Q_{hr}, and total heat generation rate Q_h under the discharge conditions of 1C, 3C, 5C and 10C. As seen in Fig. 6, Q_{hir} seems relatively even and displays a depression near the DOD of 0.5, which is due to the small change of the internal resistance of the battery (ranging from 6 to 8 mΩ). The internal resistance of the battery also shows its minimum value near DOD of 0.5 (as shown in Fig. 3). With the increase of the discharge rate, Q_{hir} rises rapidly and occupies an increasingly large proportion in the total heat generation rate, which is consistent with literature [22]. The increase of Q_{hr} displays is not obvious, which can be explained by Equations (4) and (5). Irreversible heat generation is related with the discharge current and the internal resistance of the battery. In the case of a relatively small change of internal resistance, irreversible heat generation is in direct proportion to the square of the current. The

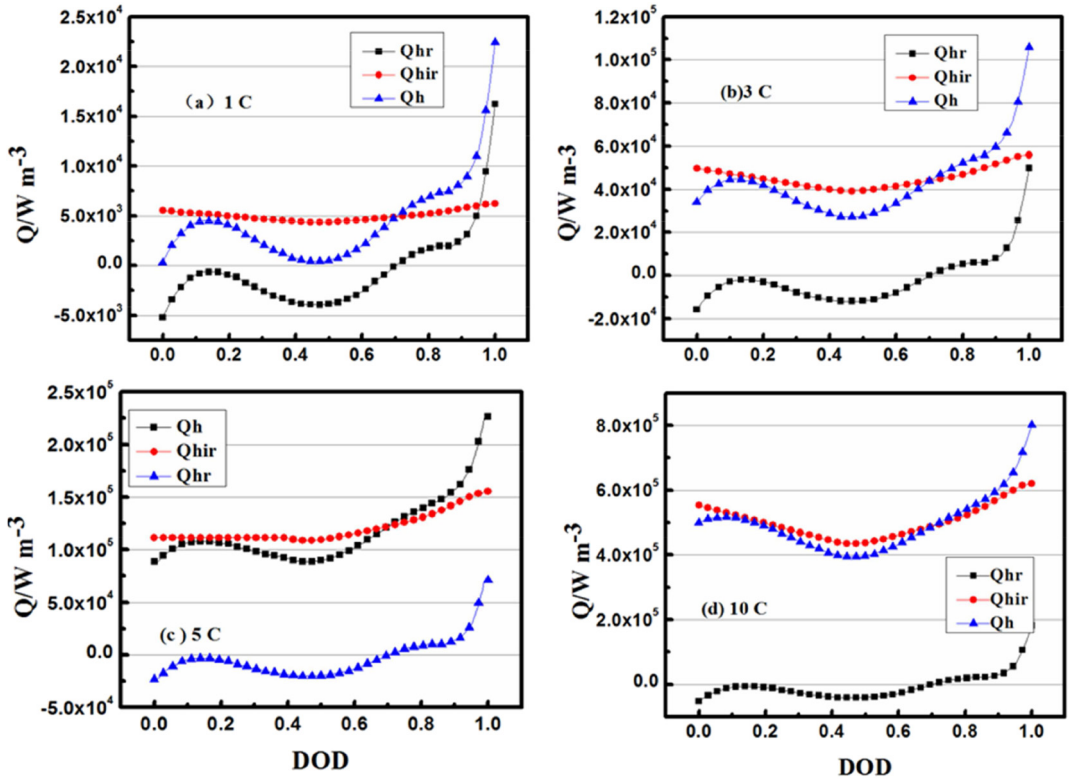

Fig. 6. Comparison of internal heat generation at different discharge current (a)1C; (b)3C; (c)5C; (d)10C.

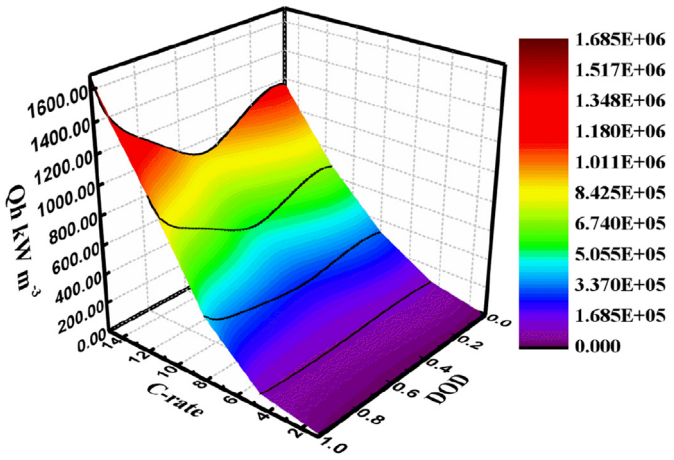

Fig. 7. The diagram of the three-dimensional relationship among the total heat generation rate, discharge rate and the depth of discharge.

chemical reaction irreversible heat is related to the discharge current, cell temperature and voltage temperature coefficient. In the case of a relatively small change of the cell temperature and voltage temperature coefficient, reversible heat is approximately in proportion to the first power of the current. When DOD is below 0.7 and chemical reversible heat generation rate Q_{hr} is less than 0, the chemical reaction is manifested by an endothermic process; when DOD is above 0.7 and Q_{hr} is greater than 0, it is manifested by an exothermic process, which is consistent with the voltage temperature coefficient of LFP aluminum-laminated battery shown in Fig. 3. When the depth of discharge is ranged between 0.2 and 0.7, the potential curve displays an endothermic peak and the related heat generation rate curve Q_{hr} displays a wave trough.

As for the heat generation, it is a function of I, T, R_{cell} and dU_{avg}/dT, we know that R and U_{avg} are both variations by the depth of discharge (DOD) as Figs. 2 and 3 depicted, then we can look the heat generation as a function of I, T and DOD, once we have fixed the initial temperature T_0, then heat generation will be refreshed due to the coupling relationship between Q and T. Therefore, on this condition, we can regard the heat generation as a function of I and DOD, and T is the only contribution that causes Q to vary spatially. Fig. 7 shows the diagram of the three-dimensional relationship among the total heat generation rate, discharge rate and the discharge depth inside the battery; it is fitted with the bivariate polynomial data and thus the binary cubic polynomial fitting function is obtained, as shown in Equation (11).

$$z = -65.3622x3 + 482798.55443y3 + 2116.21774x2y + 136750.25995xy2 + 5688.24557x2 - 1.14369e6y2 - 149184.23179xy + 16119.0284x + 710485.07516y - 82637.90799 \quad (11)$$

where, z is the total heat generation rate of the battery (the unit is W/m^3); x and y represent the discharge rate and discharge depth of the battery, respectively; the degree of fitting r^2 is 0.9953. It can be easily concluded from Equation (11) that the total heat generation rate data under different discharge rates and depths can be applied to optimize power LFP batteries and the thermal management strategy of battery pack. Actually there still exist some restrictions for Equation (11) in employment. That is, at the first place, the heat generation is calculated at a specific initial temperature, it is 300 K in this work; besides, it is suitable for continually discharging process, for other processes like uncontinually discharging or temperature changing mandatorily (eg. put into an extremely cold environment), the Equation (11) will do not work.

3.3. Influence of tab position on the heat distribution of battery cell

Fig. 8 shows the simplified model graph of 10 Ah power aluminum laminated battery cells, wherein M_nN_n ($n = 1, 2$ and 3) is a straight line perpendicular to the edge of the anode. The conductivity of anode aluminum sheet is lower than that of cathode copper sheet, and when the current passes through, the heat generation rate of anode is relatively high. Due temperature gradient along MN line is expected to be higher than that in the other region of the battery, the temperature fluctuations on MN

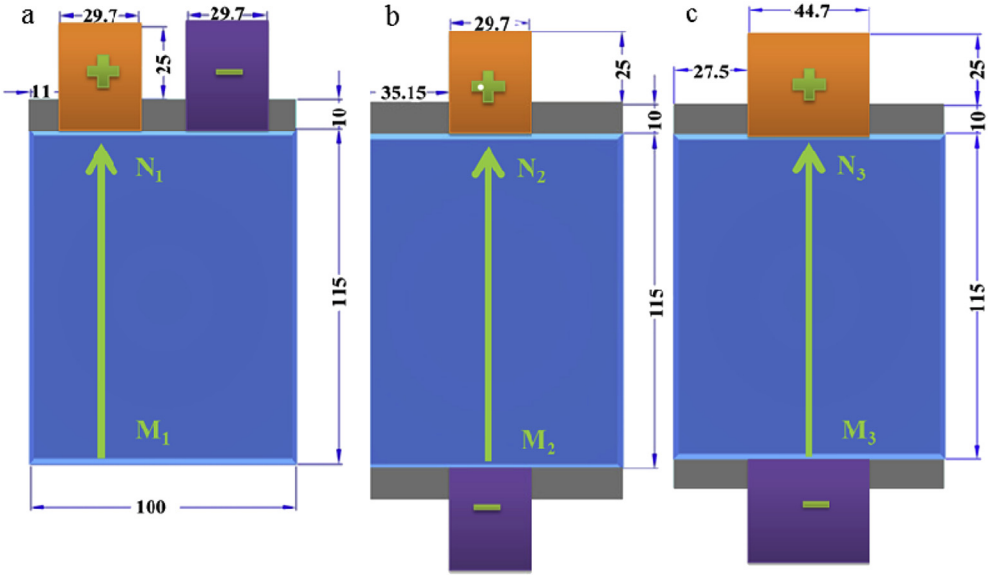

Fig. 8. The simplified model graph of 10 Ah power aluminum laminated battery cells. a. single-side tab distribution. b. double-side tab distribution. c. double-side tab distribution (*1.5).

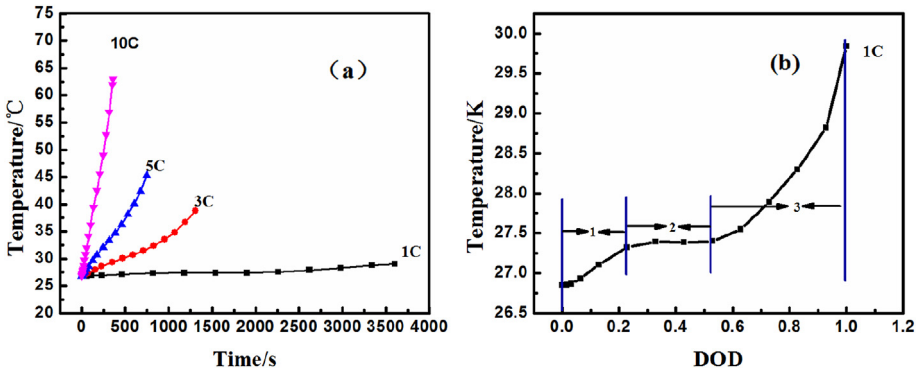

Fig. 9. (a) The temperature curve of single-side tab batteries under different rates; (b) the discharge temperature curve of single-side tab at the rate of 1C.

shows good universality and representativeness and can be adopted to investigate the cell temperature distribution [23].

Battery temperature distribution is the result of the comprehensive action of the internal heat generation and external heat dissipation, and its temperature change is not only related to the chemical reaction reversible heat generation and internal resistance irreversible heat generation, but also to the tab position. The study object is implemented with discharges of 1C, 3C, 5C and 10C (Fig. 8a), and the curves of average temperature change of the battery under natural convection condition are shown in Fig. 9.

Fig. 9a shows the temperature curve of single-side tab batteries under different rates. With the increase of the discharge rate, the mean battery temperature at the end of the discharge rises and the temperature rise curve tends to be linear. It is revealed by the

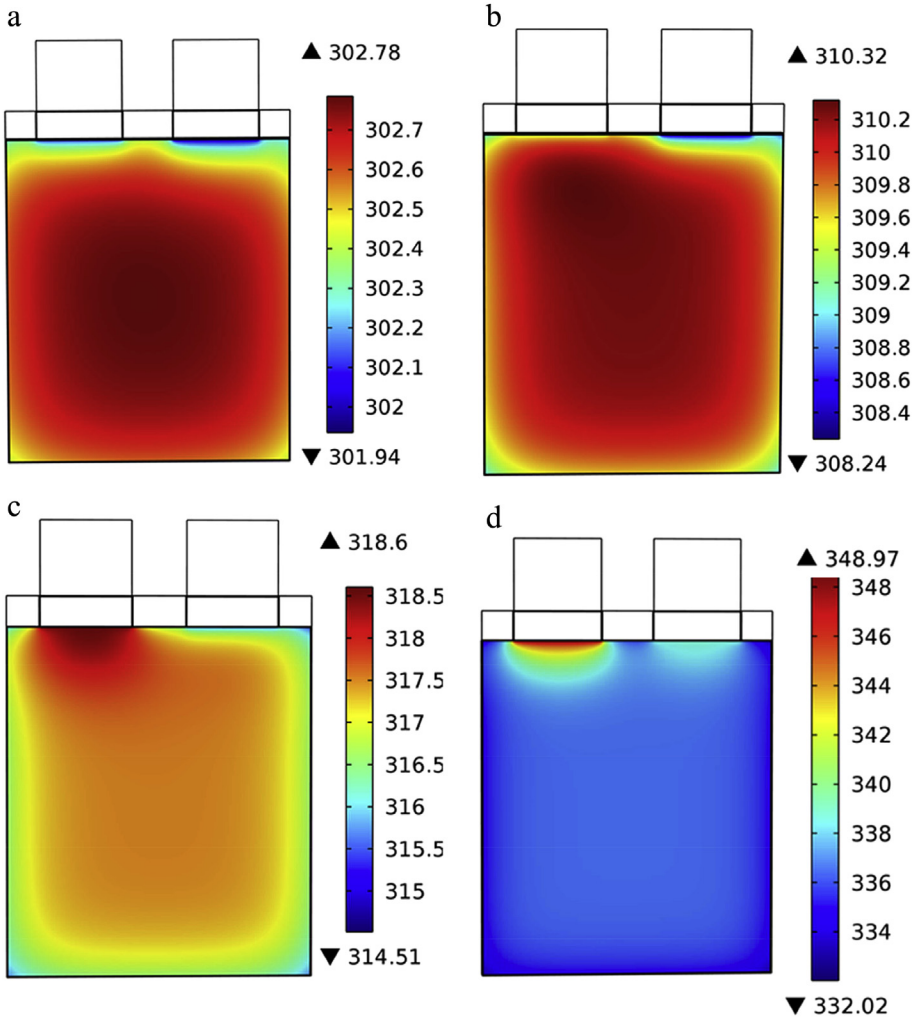

Fig. 10. The temperature distributions of the center section under different rates. (a) 1C; (b) 3C; (c) 5C; (d) 10C.

simulation that the maximum temperature at the end of the discharge is 45.5 °C, near the ceiling of acceptable temperatures required for normal operation of lithium-ion batteries. At the end of discharge of 10C, the mean temperature of cell is 63.0 °C, well beyond the temperature range required by normal operation, which would significantly reduce cycle life and battery performance in real applications. Fig. 9b provides the discharge temperature curve of single-side tab aluminum-laminated battery at the rate of 1C. It can be seen that the curve is roughly divided into three sections: when DOD is in the range 0–0.2 or 0.5–1, the curve presents an increasing trend; when DOD is in the range from 0.2 to 0.5, the temperature rise curve flattens out. As seen in Fig. 6a, the internal total heat generation rate curve Q_h presents an increasing trend when DOD is ranged from 0 to 0.2 and from 0.5 to 1, which explains that the internal total heat generation rate keeps increasing and the internal heat is gradually accumulated, thus leading to the temperature rise of the battery. The Q_h curve displays a decreasing trend when DOD is ranged from 0.2 to 0.5, which explains that the internal heat generation rate in this section decreases gradually and the accumulation of internal heat slows down. Due to the heat transfer on the surface of the battery, the internal and external heat transfer inside the battery has reached an approximate equilibrium state, without any temperature rise.

Fig. 10 presents the temperature distributions of the center section of study objects under different rates. It can be seen that, at the rate of 1C, the cell temperature is influenced by the tab to a lesser extent and the high temperature regions are concentrated in the center area; when the discharge is at the rate above 3C, due to the large current, the tab will generate a significant amount of heat and the high-temperature regions concentrate in the areas near the tabs. The thermal imagery analysis on the lithium-ion polymer battery during the discharge conducted by Keyser MA [24]. also shows the same temperature distribution trend.

In practical applications, double-side tab batteries (shown in Fig. 8b) are sometimes used in response to high rate requirements of the power system. In the case of constant tab size, the temperature of the center section is studied and the results showed that the distribution of double-side tabs drives the battery temperature to be distributed evenly and symmetrically; however, when the rate is above 3C, the high-temperature regions concentrate in the area near the anode tab. In order to solve the problem of battery temperature drift near the anode tab at high rate, tabs of the double-side tab lithium-ion batteries can be widened. Since the cross sectional areas of widened tabs are larger, when the same intensity of current passes through, the current density of tabs is reduced and the heat generation rate is decreased. Thus the influence on the distribution uniformity of cell temperature is reduced

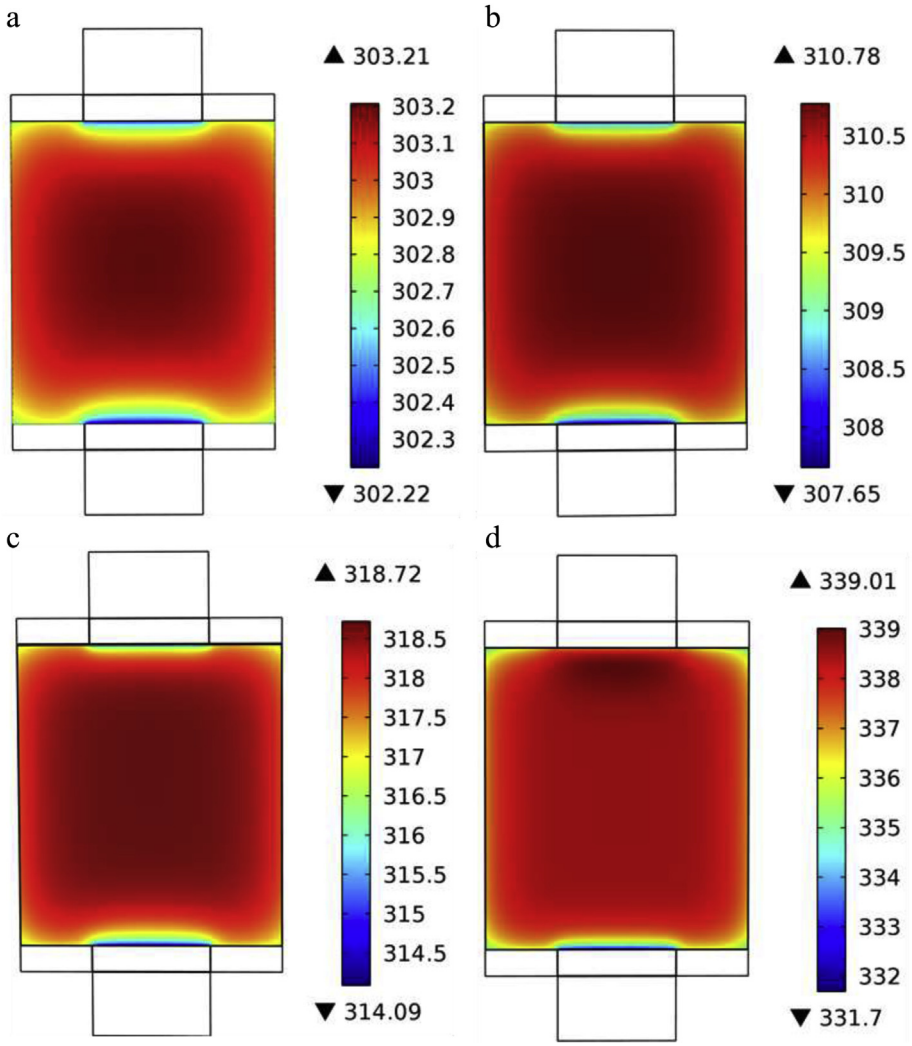

Fig. 11. The temperature distribution of battery center section at different rates. (a) 1C; (b) 3C; (c) 5C; (d) 10C (the tab is 1.5 times wider than before).

at the same time. Fig. 11 provides the temperature distribution of battery center section at different rates derived by increasing the width of the tab 1.5 times (shown in Fig. 8c). It can be seen that the cell high temperature regions at rates of 1C, 3C and 5C concentrate in the center area; additionally, the maximum temperature values of cells drop significantly at rate of 10C. To be specific, compared with the battery tab distribution shown in Fig. 8b, the maximum temperatures decreased respectively by 0.01 K, 0.09 K, 0.94 K and 11.83 K. We can therefore conclude that broadening the width of tabs can improve the distribution uniformity of battery temperature, and effectively reduce the maximum temperature of the battery. The higher the discharging rate, the greater the improvement in maximum temperature.

Fig. 12 shows the temperature change at the end of discharge at 3C, 5C, 10C on the MN line of three batteries with different tab configurations. It can be seen that the temperature of cell center area of double-side tab distribution battery is a little higher than that of single-side tab battery for the discharge rate of 3C and 5C.besides, compared with double-side tab (Fig. 8b), widening the tab size will exert a relatively small change in cell temperature at the end of discharge of the battery at 3C and 5C; But at the rate of 10C, widening the tab size will significantly decrease the temperature and make the battery temperature distribute more evenly. Above all, comparison with single-side tab, double-side tab or even widen the tabs both have little impact on temperature distributions at 3C and 5C, and their differences are visible in the temperature uniformity, especially at high discharge rate, widening the tabs will make the cell have more even temperature distribution.

While discharging at 10C, the internal temperature of the battery will exceed the normal operating temperature range. In practical applications, in order to decrease the maximum temperature of the battery and improve the internal temperature distribution of the battery, certain heat dissipation strategies are adopted, such as air cooling and oil cooling, filling of phase-change materials with larger heat capacities (PCM, phase change materials), and so on [25–27]. As we have shown, rational cooling mechanisms can be designed with respect to specific temperature distributions of batteries under different working conditions, and relevant studies can be further crystallized in future work.

4. Conclusion

A three-dimensional thermal simulation model based on finite element theory is established using 3.2 V/10 Ah LFP as the research object. In this model, the battery is assumed to be theoretically fully discharged and the battery aging caused by the internal side reaction as well as the heat generation terms during the material mixing process caused by the concentration gradient inside the battery are ignored. And then proceeded from the heat generation inside the battery, the effects on the heat distributions of the battery cells by different types of tab configurations are explored theoretically. Results show in the following: Firstly, numerical simulation plays a very important role in the research of lithium ion battery. The thermal behavior of the discharge process can be effectively simulated by coupling the dynamic changes of the battery temperature, internal resistance, and voltage temperature coefficient. Secondly, the total interior heat generation basically contains two parts: chemical reversible heat and irreversible heat. The reversible heat of the battery is manifested by the endothermic process when DOD is smaller than 0.7 and by the exothermic process when DOD is larger than 0.7. And the irreversible heat takes an increasingly dominant role with the increase of discharge rate; thirdly, comparison with single-side tab, double-side tab distribution can improve the uniformity obviously, but a little higher interior temperature than single-side tab will be found at the discharge rate of 1C, 3C, 5C. Widening the tab can greatly reduce the maximum temperature of the cell especially at high discharge rate of 10C and have more even temperature distribution.

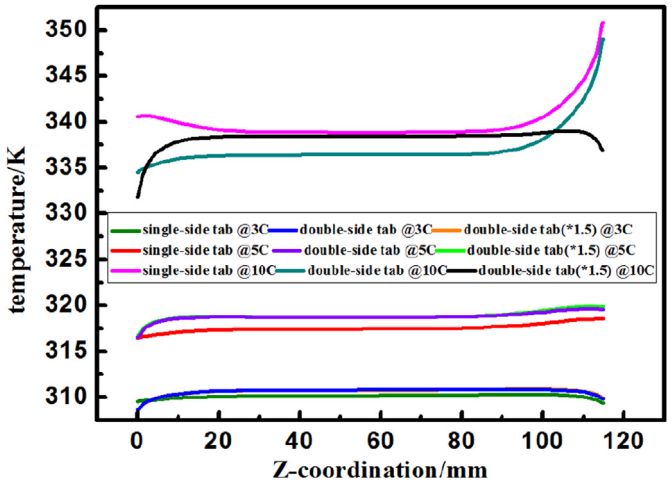

Fig. 12. Temperature variations at the end of discharge at 3C, 5C, 10C on the MN line of three batteries with different tab distributions.

Acknowledgment

This work is supported by funds from the National Natural Science Foundation of China (No. 51204211 and No. 51222403), the China Postdoctoral Science Foundation (No: 2012M521543), and the Open-End Fund for the Valuable and Precision Instruments of Central South University (CSUZC2014029) which are greatly appreciated. The authors also thank School of Energy Science and Engineering at the University of Central South University for assistance in infrared imagery.

References

[1] L. Jia, Y. Chuanzhen, Z. Xigui, et al., XRD studies on the electrode materials in the charge-discharge process of a graphite/Li($Ni_{1/3}Co_{1/3}Mn_{1/3}$)O_2 battery, Acta Phys. Sin. 58 (9) (2009) 6573–6581.
[2] N. Sato, K. Yagi, Thermal behavior analysis of nickel metal hydride batteries for electric vehicles, JSAE Rev. 21 (2) (2000) 205–211.
[3] Todd M. Bandhauer, Srinivas Garimella, Thomas F. Fuller, A critical review of thermal issues in lithium-ion batteries, J. Electrochem. Soc. 158 (3) (2011) R1–R25.
[4] D. Bernardi, E. Powlikowski, J. Newman, A general energy balance for battery systems, J. Electrochem. Soc. 132 (1) (1985) 5–12.
[5] L. Wencheng, L. Shigang, Thermal behavior of C/$LiFePO_4$ power secondary battery, Chin. J. Nonferrous Met. 22 (4) (2012) 1156–1162.
[6] T. Yiwei, J. Ming, C. Yun, et al., Estimate temperature distribution of the polymer lithium ion power battery based on the coupling relationship between electrochemistry and heat, Acta Phys. Sin. 62 (2013) 158201-1–158201-10.
[7] Z. Kai, T. Yiwei, Z. Zhong, et al., Simulation of diffusion polarization in $LiMn_2O_4$/graphite Li-ion battery during discharge process, Chin. J. Nonferrous Met. 23 (8) (2013) 2235–2246.
[8] T. Yiwei, J. Ming, L. Jie, L. Yanqing, C. Yun, L. Yexiang, Numerical analysis of distribution and evolution of reaction current density in discharge process of lithium-ion power battery, J. Electrochem. Soc. 161 (8) (2014) E1–E7.
[9] L. Jie, C. Yun, J. Ming, T. Yiwei, L. Yue, Z. Zhian, L. Yexiang, An electrochemical–thermal model based on dynamic responses for lithium iron phosphate battery, J. Power Sources 255 (2014) 130–143.
[10] S.K. Ui, B.S. Chee, K. Chisu, Effect of electrode configuration on the thermal behavior of a lithium-polymer battery, J. Power Sources 180 (2) (2008) 909–916.
[11] S.K. Ui, B.S. Chee, K. Chisu, Modeling for the scale-up of a lithium-ion polymer battery, J. Power Sources 189 (1) (2009) 841–846.
[12] S.K. Ui, Y. Jaeshin, B.S. Chee, et al., Modeling the dependence of the discharge behavior of a lithium-ion battery on the environmental temperature, J. Electrochem. Soc. 158 (5) (2011) A611–A618.
[13] Z. Wei, L. Gang, W. Chaoyang, Effect of tab design on large-format Li-ion cell performance, J. Power Sources 257 (2014) 70–79.

[14] L. Damen, J. Hassoun, M. Mastragostino, B. Scrosati, Solid-state, rechargeable Li/$LiFePO_4$ polymer battery for electric vehicle application, J. Power Sources 195 (19) (2010) 6902–6904.
[15] S.C. Chen, C.C. Wan, Y.Y. Wang, Thermal analysis of lithium-ion batteries, J. Power Sources 140 (1) (2005) 111–124.
[16] K.E. Thomas, J. Newman, Thermal modeling of porous insertion electrodes, J. Electrochem. Soc. 150 (2) (2003) A176–A192.
[17] C. Forgez, D.V. Do, G. Friedrich, M. Morcrette, C. Delacourt, Thermal modeling of a cylindrical $LiFePO_4$/graphite lithium-ion battery, J. Power Sources 195 (2010) 2961–2968.
[18] K. Onda, H. Kameyama, T. Hanamoto, et al., Experimental study on heat generation behavior of small lithium-ion secondary batteries, J. Electrochem. Soc. 150 (3) (2003) A285–A291.
[19] L. Chengtao, L. Teng, C. Quanshi, Analysis of the heat dissipation capability influence factors of $LiMn_2O_4$-based lithium-ion power battery, Acta Armamentar II 31 (1) (2010) 89–93.
[20] A. Pesaran, A. Vlahinos, D. Bharathan, in: The 24th International Battery Seminar & Exhibit March 13–16, 2006. Fort Lauderdale, Florida, NREL/PR-540-39503.
[21] G. Guo, B. Long, B. Cheng, et al., Three-dimensional thermal finite element modeling of lithium-ion battery in thermal abuse application, J. Power Sources 195 (8) (2010) 2393–2398.
[22] D.H. Jeon, S.M. Baek, Thermal modeling of cylindrical lithium ion battery during discharge cycle, Energy Convers. Manag. 52 (2011) 2973–2981.
[23] Ui Seong Kim, Jaeshin Yi, Chee Burm Shin, Taeyoung Han, Seongyong Park, Modelling the thermal behaviour of a lithium-ion battery during charge, J. Power Sources 196 (11) (2011) 5115–5121.
[24] M.A. Keyser, A. Pesaran, M. Mihalic, Thermal characterization of advanced lithium-ion polymer cells, in: Third Advanced Automotive Battery Conference, June 2003.
[25] M.M. Farid, A.M. Khudhair, S.A.K. Razack, et al., A review on phase change energy storage: materials and applications, Energy Convers. Manag. 45 (9–10) (2004) 1597–1615.
[26] R. Kizilel, A. Lateef, R. Sabbah, et al., Passive control of temperature excursion and uniformity in high-energy Li-ion battery packs at high current and ambient temperature, J. Power Sources 183 (1) (2008) 370–375.
[27] R. Sabbah, R. Kizilel, J.R. Selman, et al., Active (air-cooled) vs. passive (phase change material) thermal management of high power lithium-ion packs: limitation of temperature rise and uniformity of temperature distribution, J. Power Sources 182 (2) (2008) 630–638.